SUPPLEMENTAL MATERIAL

METHODS

This retrospective series included clinical, pathological and laboratory data from 16 patients with confirmed SARS-CoV-2 infection who were autopsied in our institution. Consented autopsies were performed following all recommended security measures, as previously reported.[1] The Research Ethics Committee approved the study (reference: Necropsias_Covid19) and waived the need for informed consent for immunohistochemical studies on tissue samples, which were managed through the Hospital Universitario Ramón y Cajal-IRYCIS Biobank. This cohort did not include healthy or non-COVID control subjects.

Histopathological evaluation

Samples from the five pulmonary lobes were taken in all patients. All histological evaluations were blinded to clinical data. The histopathological classification of the diffuse alveolar damage (DAD) lesions was performed according to Li et al:[2] organising DAD demonstrated loose organising fibroblastic tissue consisting of polypoid plugs within distal air spaces or rounded nodular foci of loose myxoid fibrosis centred on alveolar ducts, whereas the fibrosing DAD pattern showed the presence of dense interstitial fibrous tissue in the form of alveolar duct fibrosis or diffuse thickening of alveolar walls.

The semiquantitative assessment of organizing and fibrosing DAD was performed on haematoxylin and eosin (H&E) stained sections (2 sections from each lung lobe, 160 sections in total). The percentage of area occupied by organizing/fibrotic

lesions in each lobe was recorded, and the results for each patient was presented as the mean ± the standard deviation of the 5 lobes (10 sections per patient).

Immunohistochemical methods

EnVision FLEX/HRP system was used for immunohistochemistry (Agilent, Santa Clara, CA). For dual immunostainings, EnVision FLEX DAB+Chromogen (Agilent) was used to obtain the brown colour and EnVision FLEX HRP Magenta Chromogen was used to obtain the magenta colour.

To evaluate lung vascularization, the expression of CD34 (clone QBEnd10 ready to use, Agilent), CD31 (clone JC70A ready to use, Agilent), and endothelial vascular cadherin (VE-cadherin) (clone E6N/A, 1/400, Cell Signalling) was analysed on sections taken from all five lung lobes in each patient.

Since the type of vascular alterations, we observed in this series has not been previously quantitatively evaluated, we defined a vascular score (VS), which was easily reproducible, based on both the size and the number of lesions evaluated on CD34 sections (see Material and Methods section in the main text).

In order to perform additional immunohistochemical analysis, among all evaluated slides, we selected 12 areas, from 12 different patients, that included all the range of lesions described: normal appearing lung (n=3), VS1 (n=3), VS2 (n=3), and VS3 (n=3). PDGFR-β (clone Y92, 1/600, Abcam) was used to evaluate the presence pericytes. Smooth muscle actin (SMA) (clone HHF35 ready to use, Agilent) was used to evaluate the presence of myofibroblast and pericytes. VEGF (clone VG1, 1/200, Agilent) expression was analysed as a proangiogenic factor. Dual immunohistochemistry for CD34/CK18 (clone EP30 ready to use, Agilent) was

performed to evaluate the relationship between vascular proliferations and the alveolar lining. Dual immunohistochemistry for CD34/SMA was performed to evaluate the presence of pericytes in areas of vascular proliferation. Dual immunohistochemistry for CD34/Ki67 (clone QBEnd10 and clone MIB-1, ready to use, Agilent) was used to evaluate proliferation in vascular areas. Dual CD34/CD68 (clone QBEnd10 and clone PG_M1, ready to use, Agilent) immunohistochemistry was used to evaluate the presence of macrophages around vascular areas.

All immunostained slides included, in addition to lung tissue, a section of an appendix as positive control. Substitution of the primary antibody by an isotype-specific immunoglobulin was used as negative control in selected cases.

Initial histological evaluation of lung samples was independently done by three pathologists (BPM, ICB, JP). Afterwards, they were reviewed together with two expert pulmonary pathologists (AB, MGC), agreeing the definitive histopathological and vascular scores for each patient.

Statistical analysis

Statistical analyses were conducted with R3.6.2.[3] Correlations were evaluated by Spearman's coefficient and means comparisons were tested by Mann-Whitney-U. A two-sided P less than 0.05 was considered statistically significant.

RESULTS

This series included 13 men and 3 women. Clinical, laboratory, pathological and pulmonary functional characteristics of patients are shown in Supplementary Table 1.

Supplementary Table 1

Clinical, laboratory, pathological and pulmonary function characteristics of patients.

Demographics and clinical characteristics			**Total number of observations**
Age, years	Median (IQR) Min, max	67.50 (14.75) 52, 91	16
Gender, n (%)	Male	13 (81)	16
Weight, kg	Median (IQR) Min, max	80 (19.88) 53, 109	14
DM, n (%)		1 (6)	16
Hypertension, n (%)		7 (44)	16
Patients admitted to ICU, n (%)		13 (81)	16
Hospitalization days	Median (IQR) Min, max	30 (12.25) 3, 69	16
ICU days	Median (IQR) Min, max	23.50 (19.25) 0, 49	16
Mechanical ventilation n (%)		13 (81.20)	16
Laboratory test at admission (normal values)			
Oxygen saturation (>96), %	Median (IQR) Min, max	87.50 (14.50) 70, 99	16
White cell count (4-11), $10^3/\mu L$	Median (IQR) Min, max	9.62 (7.62) 0.01, 18.90	16
Neutrophils, %	Median (IQR) Min, max	85.75 (18.66) 18.20, 96.90	16
Lymphocytes (1-4.5), $10^3/\mu L$	Median (IQR) Min, max	0.96 (0.52) 0, 1.45	16

Creatinine (0.3-1.3), mg/dL	Median (IQR)	0.88 (0.17)	16
	Min, max	0.48, 2.82	
CRP (0-5), mg/L	Median (IQR)	195.85 (155.93)	16
	Min, max	9.30, 349	
Ferritin (20-300), ng/mL	Median (IQR)	1445.18 (1211.88)	14
	Min, max	142.95, 2741.18	
Lactate dehydrogenase (140-240), U/L	Median (IQR)	477 (253.25)	16
	Min, max	270, 987	
Platelets (140-400), $10^3/\mu L$	Median (IQR)	217.50 (102)	16
	Min, max	22.30, 479	
Fibrinogen (150-400), mg/dL	Median (IQR)	740 (158.35)	16
	Min, max	295.10, 740	
APTT (76-128), %	Median (IQR)	83.90 (15.93)	16
	Min, max	16.10, 102.90	
PT (9.7-12.6), s	Median (IQR)	12.20 (0.93)	16
	Min, max	11.10, 49.20	
D-dimer (0-500), ng/mL	Median (IQR)	1160 (6312.50)	15
	Min, max	258, 14992	
Troponin (0-0.1), ng/mL	Median (IQR)	0 (0.10)	16
	Min, max	0, 0.80	
Natriuretic peptide, pg/mL	Median (IQR)	86.90 (108.27)	15
	Min, max	19, 2288	
IL6 at admission, pg/mL	Median (IQR)	101.61 (124.82)	14
	Min, max	1.27, 589	
Highest IL6, pg/mL	Median (IQR)	1947.46 (3835.08)	14
	Min, max	1.27, 14493.41	
Highest IL10, pg/mL	Median (IQR)	7.87 (5.13)	14
	Min, max	0.50, 54.44	

Highest IL12, pg/mL	Median (IQR) Min, max	1.32 (3.03) 0.26, 6.66	14
Pathologic findings			
Normal lung, %	Median (IQR) Min, max	0 (0) 0, 30	16
Exudative DAD, %	Median (IQR) Min, max	43 (35.25) 2, 92	16
Proliferative/Organizing DAD, %	Median (IQR) Min, max	39 (31) 0, 90	16
Fibrotic DAD, %	Median (IQR) Min, max	8 (14) 0, 39	16
Acute bronchopneumonia, n (%)		9 (56.30)	16
Vascular thrombi, n (%)		12 (75)	16
Endothelialitis, n (%)		13 (81.25)	16
Vascular Score, n (%)	High (>5)	8 (50)	16
Pulmonary function			
Initial Dynamic compliance, ml/cm H20	Median (IQR) Min, max	31 (16) 12, 71	13
Initial PaO2/FIO2	Median (IQR) Min, max	118 (124) 36, 250	13
Initial Ventilation Ratio	Median (IQR) Min, max	2 (1.40) 1.14, 4	13
Final Dynamic compliance, ml/cm H20	Median (IQR) Min, max	26 (30) 5, 60	13
Final PaO2/FIO2	Median (IQR) Min, max	83 (36) 50, 135	13
Final Ventilation Ratio	Median (IQR) Min, max	2.50 (0.80) 1.40, 5.20	13

Histopathological analysis revealed severe diffuse alveolar damage (DAD) in all but one patient, where only occasional areas of hyaline membranes were found. The predominant lung pattern was DAD in fibroproliferative stage, but exudative or fibrotic lesions were also present in different proportions in each patient (Supplementary Figure 1A to 1C). The most advanced areas of fibrosis were found in subpleural location (Supplementary Figure 2A). In these areas, decreased vascularisation was evident after immunohistochemical analysis with endothelial markers (Supplementary Figure 2C). Endothelialitis was observed in 13 patients (81.25%), vascular thrombi (Supplementary Figure 1D) in 12 patients (75%), and associated acute bronchopneumonia in 9 patients (56.3%).

PDGFR-β was homogeneously expressed in alveolar septa and in vascular lesions, indicating the presence of pericytes (Supplementary Figures 3B and 3C). Regarding Ki67, we observed variable expression among vascular lesions. Most glomeruloid or coalescent lesions showed 1% to 5% of Ki67-positive endothelial cells. However, in some areas, the number of Ki67-positive endothelial cells reached up to 15% (Supplementary figure 4A and 4B).

Macrophages were the most abundant inflammatory cells in the alveoli, and they were frequently observed in close spatial relationship with vascular lesions (Supplementary Figure 5A). Mild VEGF expression was observed in alveolar macrophages in some, but not all analysed areas (Supplementary Figure 5B). Only in one VS2 lesion out of the 9 lesions analysed with a VS>0, VEGF expression was detected in cells of the glomeruloid vascular structures, which appeared to correspond to endothelial cells (Supplementary Figure 5C).

No correlations were found between VS and any of the clinicopathological variables, except for age, where VS increased with the patient age (Supplementary Figure 6). We did not find statistically significant differences between patients with high and low VS in body weight (81.29±17.61 vs 79.93±15.92 kg), hospital length of stay (33.88±19.90 vs 27.38±12.35 days), ferritin (1270.92±633.21 vs 1492±1039.60 ng/ml), D-dimer (3188.71±3999.25 vs 4114.38 ± 5222.82 ng/ml), highest IL-6 (2074.48±2865.53 vs 4564.12±4919.62 pg/ml), highest IL-10 (6.32±3.53 vs 14.69±17.79 pg/ml), and highest IL-12 (2.40±1.95 vs 2.44±2.38 pg/ml). Regarding pathological features, we did not find statistically significant differences between patients with high and low VS in proliferative (36.00±21.86 vs 52±25.79 %) nor fibrotic (10.25±11.23 vs 13.13±12.35 %) DAD lesions.

DISCUSSION

The vascular nature of the lesions we describe in this study was confirmed by the expression of three endothelial markers: CD34, CD31, and VE-cadherin. Although CD34 and CD31 are also expressed by other cell types, they are routinely used for the diagnosis of vascular lesions.[4] VE-cadherin is a specific endothelial molecule that mediates adhesion of endothelial cells at adherens junctions. In addition, we were able to demonstrate that these vascular proliferations also expressed PDGFR-β, a characteristic marker of pericytes. In addition, although SMA is not specific of pericytes, their perivascular distribution, including SMA-positive cells in sections analysed by dual CD34/SMA, suggested their pericyte differentiation.

We observed PDGFR-β and SMA-positive cells in the alveolar septa of normal-appearing lung and in areas of initial viral pneumonitis. These results differed from those reported by Cardot-Leccia et al,[5] who suggested a decrease in pericytes in

alveolar capillaries in COVID-19 lungs. However, these results, which have been questioned by some authors,[6] were based on the analysis of biopsies taken in just two patients. Since no clinical, analytical, nor pathological data of these patients were reported, we cannot determine whether differences between both series were due to clinicopathological differences or to variances in the methodology used.

Our dual immunostaining analysis with CD34/Ki67 indicated that endothelial proliferation existed in vascular lesions, although it was variable among areas. Two types of angiogenesis have been described in different lung pathologies.[7–9] Sprouting angiogenesis is characterized by sprouts composed by proliferating endothelial cells, whereas intussusceptive angiogenesis is a rapid process of intravascular septation that produces two lumens from a single vessel within minutes without requiring active proliferation of endothelial cells. Intussusceptive pillar, the typical structures of intussusceptive angiogenesis, are not seen by light microscopy but are identifiable by corrosion casting and scanning electron microscopy. By using these techniques, Ackerman et al.[8] demonstrated that both intussusceptive and sprouting angiogenesis were increased in COVID-19 patients.

As an exploratory approach, we analysed the expression of the proangiogenic factor VEGF, which is elevated in the plasma of COVID-19 patients compared to controls.[10] We observed mild VEGF expression in some intra-alveolar macrophages, the type of inflammatory cells most abundant in the lung of these patients, frequently located in close spatial relation with vascular lesions. Interestingly, only in one of the vascular lesions evaluated for VEGF expression we observed immunostaining in the endothelial cells of glomeruloid structures, suggesting local autocrine signalling.[11]

The differential diagnosis of the vascular proliferation here reported included areas of poor alveolar expansion and collapse, foci of granulation tissue in the context of acute or organizing pneumonia, and pulmonary capillary hemangiomatosis (PCH). Our dual CD34/CK18 immunohistochemical study clearly demonstrated that glomeruloid lesions were not the results of apposition of collapsed septa, since those vascular proliferations did not contain entrapped epithelial cells. In more advanced stages, confluent lesions replaced alveolar spaces.

Although acute and/or organizing pneumonia could be postulated as causes for focal increase in capillaries due to granulation tissue formation, vascular proliferations here reported lacked the characteristic fibroinflammatory stroma of granulation tissue.

The hallmark histological feature of PCH is abnormal alveolar capillary proliferation, defined as $\geqslant$2 rows of capillaries within the interstitium of the alveolar walls. In PCH, alveolar septa are thickened with dilated and/or multiplication of capillaries.[12] In contrast, vascular proliferations in most COVID-19 patients in this series were formed by multiple capillary lumens that protruded, occupied, or replaced the alveolar space.

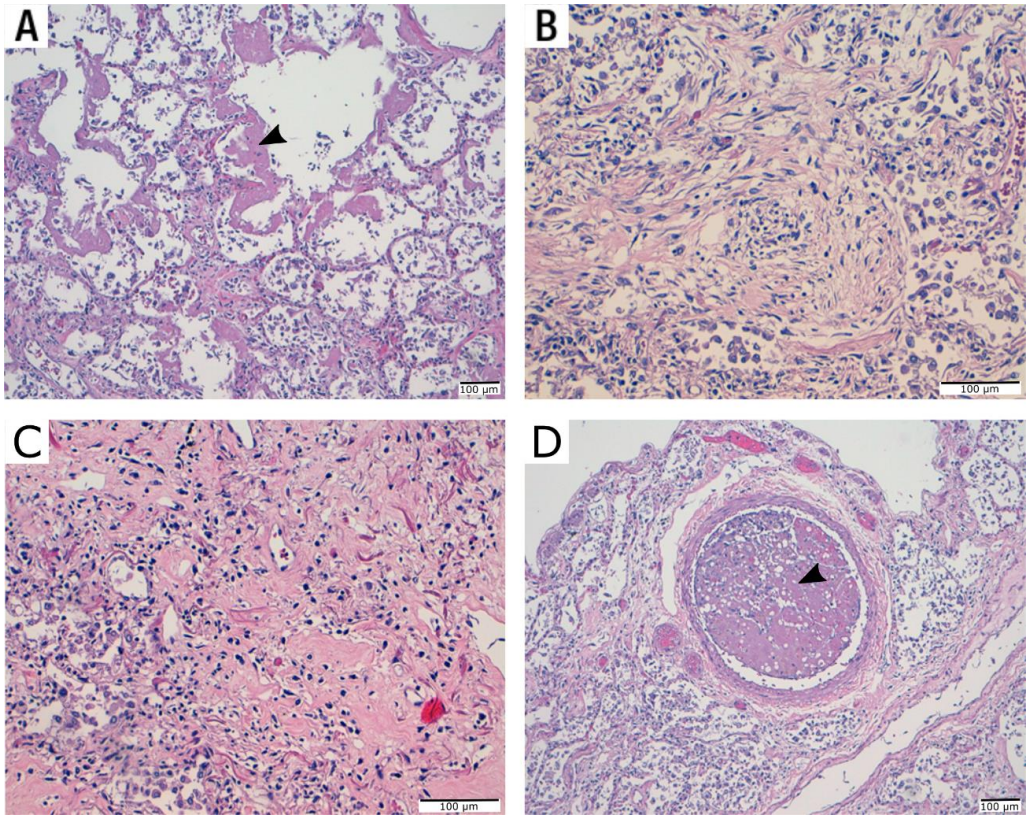

Supplementary Figure 1. (A) Hyaline membranes in exudative DAD (arrow head). (B) Proliferative/organizing phase in DAD. (C) Fibrotic phase in DAD. (D) Thrombus in medium size vessel (arrow head).

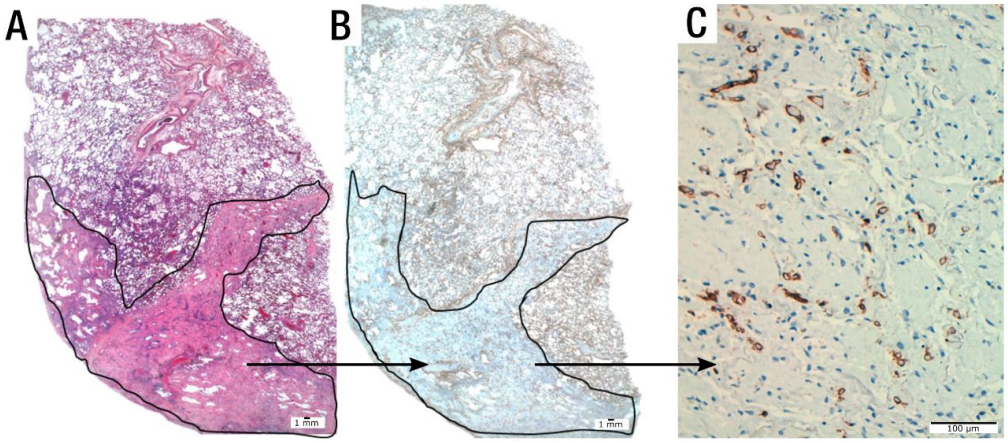

Supplementary Figure 2. (A) Wedge-shaped fibrotic subpleural area showing, in contrast with Figure 2, low vascular density (H&E). (B) CD34 staining panoramic view. (C) CD34 staining.

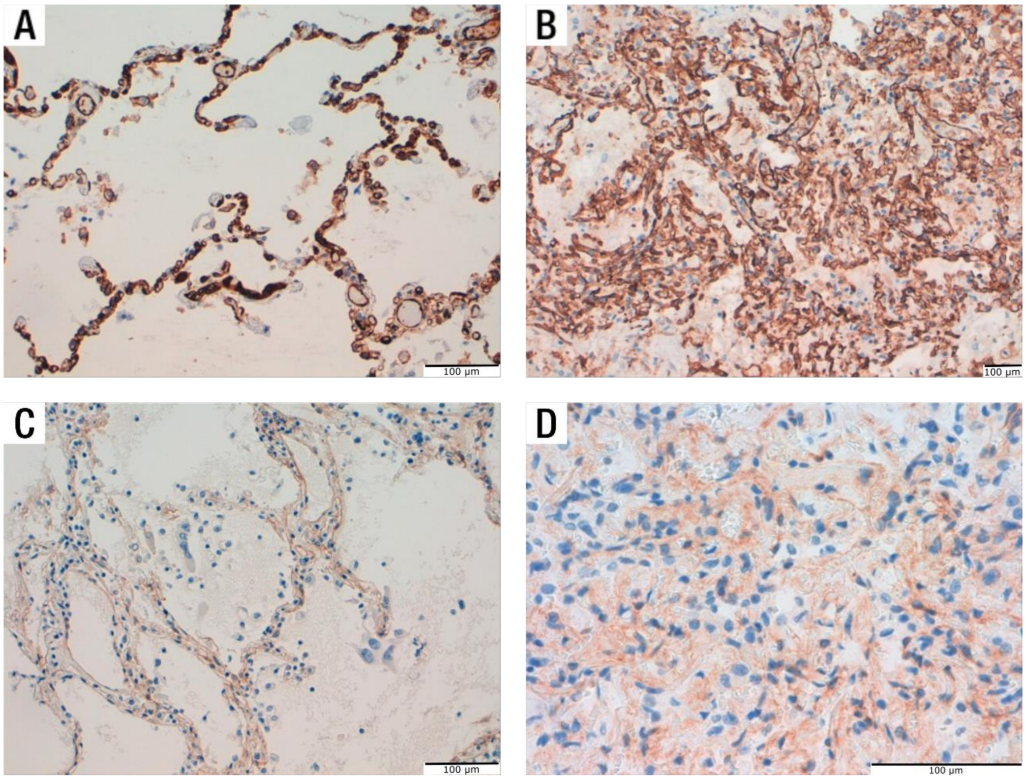

Supplementary Figure 3. (A) CD31 expression in the alveolar septa of lung areas with minimal pulmonary changes. (B) CD31 expression in a coalescent vascular lesion (VS3). (C) Homogeneous PDGFR-β expression in the alveolar septa of a lung area with mild pulmonary lesions. Note hyperplastic desquamated pneumocytes and mild inflammatory septal infiltrates. (D) PDGFR-β expression in the same coalescent vascular lesion depicted in B.

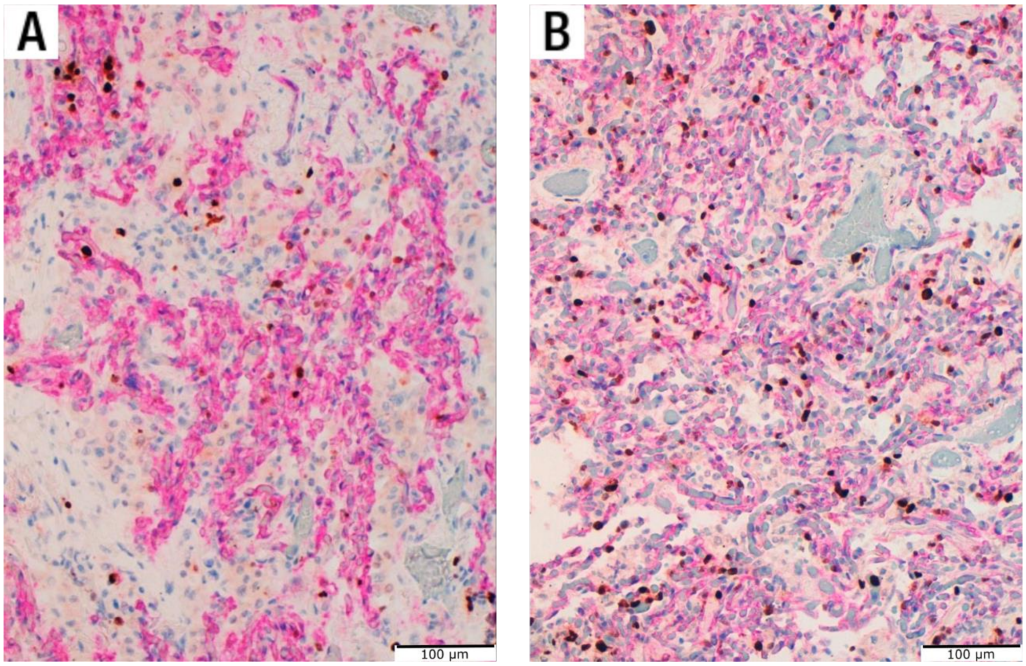

Supplementary Figure 4. Dual immunostaining of CD34 (magenta) and Ki67 (brown) in vascular lesions showing low (A) and moderate (B) proliferating activity.

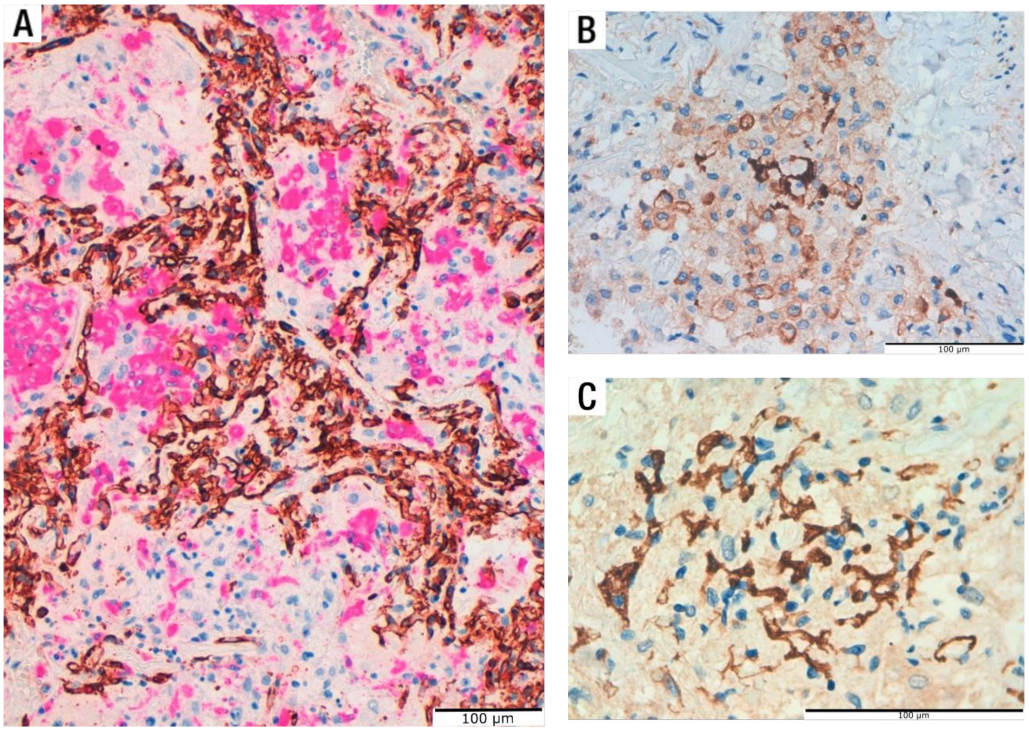

Supplementary Figure 5. (A) Dual immunostaining of CD34 (brown) and CD68 (magenta) showing the proximity of macrophages to vascular lesions. (B) VEGF expression in alveolar macrophages. (C) VEGF expression in a glomeruloid vascular lesion.

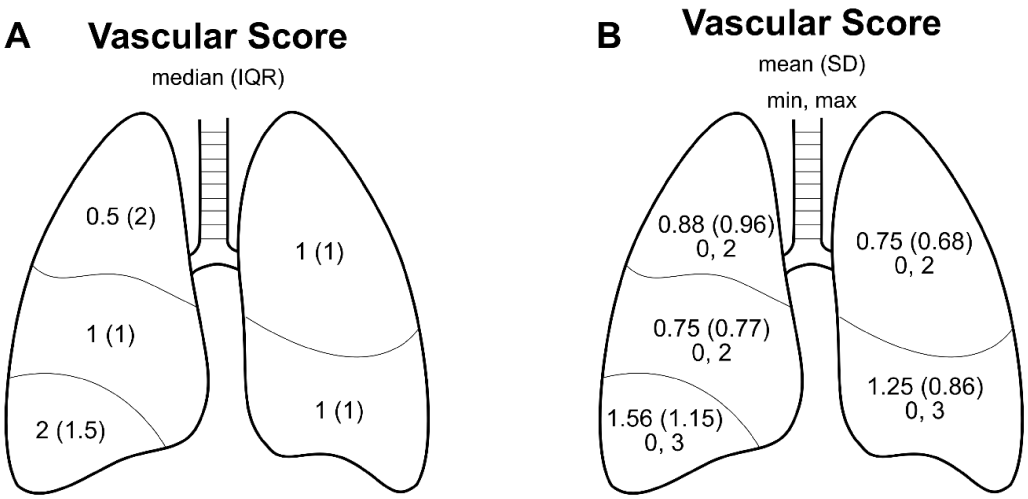

Supplementary Figure 6. Distribution vascular score (VS) across the different pulmonary lobes. (A) VS expresses as median and interquartile range (IQR). (B) VS expressed as mean, standard deviation (SD) and minimum and maximum values.

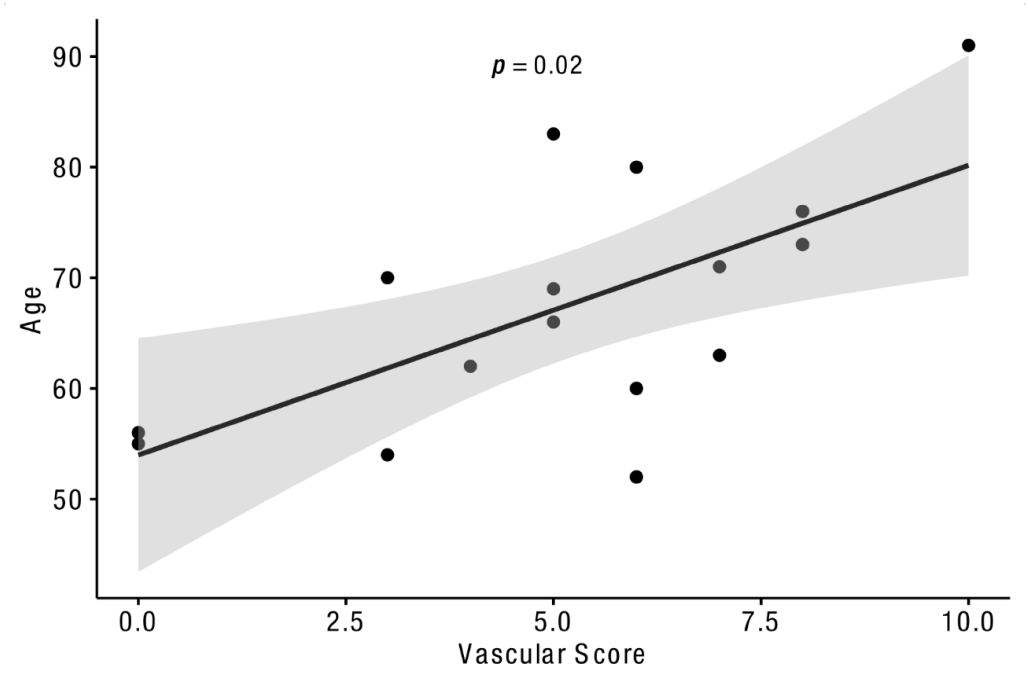

Supplementary Figure 7. Correlation between age and Vascular Score (r=0.58) with 95% confidence intervals.

REFERENCES

1 The first COVID-19 autopsy in Spain performed during the early stages of the pandemic. *Rev Esp Patol* 2020;**53**:182–7. doi:10.1016/j.patol.2020.05.004

2 Li Y, Wu J, Wang S, *et al.* Progression to fibrosing diffuse alveolar damage in a series of 30 minimally invasive autopsies with COVID-19 pneumonia in Wuhan, China. *Histopathology*;**n/a**. doi:https://doi.org/10.1111/his.14249

3 *R Core Team (2019). R: A language and environment for statistical computing. R Foundation for Statistical Computing, Vienna, Austria. URL https://www.R-project.org/*.

4 Dabbs DJ. *Diagnostic Immunohistochemistry: Theranostic and Genomic Applications.* Philadelphia: : Elsevier Health Sciences 2017. http://public.ebookcentral.proquest.com/choice/publicfullrecord.aspx?p=5253011 (accessed 26 Jan 2021).

5 Cardot-Leccia N, Hubiche T, Dellamonica J, *et al.* Pericyte alteration sheds light on micro-vasculopathy in COVID-19 infection. *Intensive Care Med* 2020;**46**:1777–8. doi:10.1007/s00134-020-06147-7

6 Jain A, Doyle DJ. Apoptosis and pericyte loss in alveolar capillaries in COVID-19 infection: choice of markers matters. *Intensive Care Med* 2020;:1–2. doi:10.1007/s00134-020-06208-x

7 Ackermann M, Stark H, Neubert L, *et al.* Morphomolecular motifs of pulmonary neoangiogenesis in interstitial lung diseases. *Eur Respir J* 2020;**55**. doi:10.1183/13993003.00933-2019

8 Ackermann M, Verleden SE, Kuehnel M, *et al.* Pulmonary Vascular Endothelialitis, Thrombosis, and Angiogenesis in Covid-19. *N Engl J Med* 2020;**383**:120–8. doi:10.1056/NEJMoa2015432

9 Ackermann M, Mentzer SJ, Kolb M, *et al.* Inflammation and Intussusceptive Angiogenesis in COVID-19: everything in and out of Flow. *Eur Respir J* 2020;:2003147. doi:10.1183/13993003.03147-2020

10 Pine AB, Meizlish ML, Goshua G, *et al.* Circulating markers of angiogenesis and endotheliopathy in COVID-19. *Pulm Circ* 2020;**10**:204589402096654. doi:10.1177/2045894020966547

11 Lee S, Chen TT, Barber CL, *et al.* Autocrine VEGF Signaling Is Required for Vascular Homeostasis. *Cell* 2007;**130**:691–703. doi:10.1016/j.cell.2007.06.054

12 Weatherald J, Dorfmüller P, Perros F, *et al.* Pulmonary capillary haemangiomatosis: a distinct entity? *Eur Respir Rev* 2020;**29**:190168. doi:10.1183/16000617.0168-2019